Journal of Engineering Sciences

Vol 11, Issue 9,SEP /2020

ISSN NO:0377-9254

ANALYSIS OF A NOVEL DVR -ESS-WIND ENERGY CONVERSION SYSTEM BY USING FUZZY LOGIC CONTROLLER

D.Rasool[1], Dr.G.V.Marutheswar[2]

[1]*M.Tech, Dept. of EEE, SVUCE, Sri Venkateswara University, Tirupati, India*

Email:rasool.1612@gmail.com

[2]*Professor, Dept. of EEE, SVUCE, Sri Venkateswara University, Tirupati, India*

Email:marutheswargv@rediff.com

***Abstract*— A novel double fed induction generator (DFIG)-based wind-energy conversion system (WECS) by using fuzzy logic controller, which incorporates a dynamic voltage restorer (DVR) and energy storage system (ESS). The DVR is in series with the output terminal of wind turbine generator (WTG) and parallel to the dc link of the WTG with the ESS. The DVR is in series with the output terminal of a wind turbine generator (WTG) and parallel to the dc link of the WTG with the ESS. The proposed fuzzy logic control scheme of WECS is designed to suppress wind power fluctuations and compensate grid voltage disturbances, improve the fault ride through (FRT) capability and wind power penetration level. The performance of WECS using PI control was investigated and compared with the proposed fuzzy logic control scheme. The results of THD using fuzzy logic control demonstrate its superiority over PI control scheme and both the steady state and dynamic response are shown.**

***Keywords*— Double-fed induction generator, energy storage system, dynamic voltage restorer, wind power fluctuations, fuzzy logic controller, total Harmonic Distortion (THD).**

1. INTRODUCTION

The fast development of wind power has brought about expanded consideration regarding wind-energy generation advancements [1]. Right now, there are fundamentally four kinds of wind turbine generators (WTGs) [2]. The most well-known WTG is the double fed induction generator (DFIG) based WTG (DFIG-WTG), which combines the benefits of traditional WTG plans and can give around ±40% speed change, boosting the measure of wind energy captured [3]. In any case, further improvement of this wind energy generation innovation is severely limited by two significant elements: 1) wind power oscillations, which are caused by discontinuous and stochastic wind speed and can bring about deviations of grid frequency and voltage, influencing the stability and power quality of grid activity [4]; 2) the fault ride through (FRT) ability, which is required by most grid codes to endure voltage dips at WTG's terminal and stay associated with the grid to help voltage and frequency during and post-fault, individually [5][6]. A few techniques have been proposed to stifle wind power changes. In [7][8], the pitch angle control is proposed to accomplish flicker mitigation and stable output power level. In [9], the utilization of turbine inertia for power smoothing is talked about. In [10], the capacity of voltage source converters to control the dynamic power output of WTGs is additionally received to smoothen power variances. On the other hand, the capacity and control range of these strategies are imperfect for the reduced wind power gaining. As another option, energy storage systems (ESSs) have been all around considered [11][12]. They not only can smoothen active power fluctuations but also can regulate reactive power. Besides, the capacity of ESSs to keep up the most extreme wind power obtaining of WTGs has indicated application possibilities. Then again, it has been demonstrated that DFIG-WTGs show risky FRT performance compared with other types of WTGs [5]. It suffers high sensitivity to grid voltage disturbances.

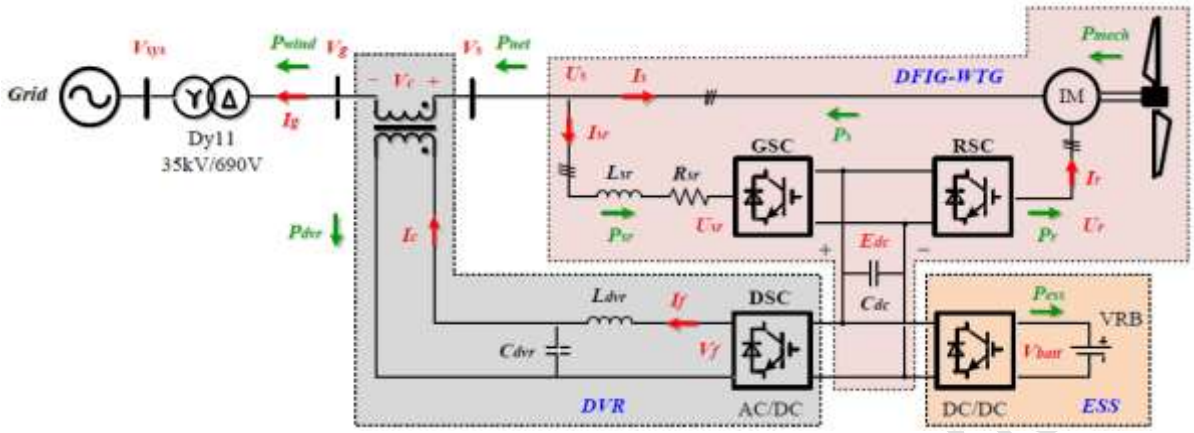

Fig. 1 Structure of the novel DVR-ESS-embedded WECS

During grid faults, the DFIG's rotor may experience damaging over current, the DC link voltage may exceed allowable limit, and the torque oscillation may reduce life time of the drive [7]. Merging the advantages of ESS and DVR, a novel DFIG based wind energy conversion system (WECS) is proposed, where a DVR is designed in series at the WTG's terminal and in parallel to DC link of the WTG with ESS. This structure is based on the adjustment of the system topology in [15] and it has the following benefits: 1) During normal operation, the ESS can absorb surplus power and release it when required to smoothen the output power of the WECS. Thus, the wind power oscillations can be greatly suppressed and the wind power penetration level in power grid can be improved. 2) Under fault conditions, the DVR can rapidly compensate symmetrical and asymmetrical voltage dips; hence, the voltage at the WTG's terminal is maintained and the WTG remains in operation. Further, the ESS in this case will store the blocked wind power for further potential fluctuation mitigation. In [16], although the DVR and the ESS are very much structured, the GSC in WECS will still experience the effects of grid voltage unsettling influences. Thus, contrasted and these arrangements, this novel structure could be exceptionally appealing. To start with, in this examination, each converter inside the proposed WECS is designed for a specific control function to avoid interference and unexpected transients. Also, the DVR is associated at the terminal of the WTG and it can prevent the WTG from being influenced by grid faults.

2. MODELING OF THE DVR-ESS-EMBEDDED WECS

The proposed novel WECS is composed of three parts: the DFIG-WTG, the DVR and the ESS, as depicted in Fig. 1. The DVR is in series connection at the WTG's terminal. Besides, both the DVR and the ESS are connected in parallel to the dc link of the WTG.

2.1. DFIG -WTG

2.1.1. WIND TURBINE: The mechanical power P_{mech} captured from wind energy with the wind turbine depends on the power coefficient $C_p(\lambda,\beta)$ and the wind speed V_w

$$P_{mech} = \frac{\rho}{2} * A_r * C_p(\lambda,\beta) * V_W^3 \qquad (1)$$

Where ρ is the air density, A_r is the area swept by the rotor blades, λ is the tip-speed-ratio and β the blade pitch angle.

2.1.2. DFIG: Basically, the stator of the DFIG is directly linked to the grid and the rotor slip-rings are connected to the grid through the partially rated back-to-back converter. The operating principle of a DFIG can be analyzed using the classic theory of rotating fields and the well-known d-q model, where the q-axis is assumed to be 90° ahead of the d-axis in the direction of rotation, and the positive current directions are defined as feeding the generator.

The reduced order DFIG model in per unit is obtained below.
Stator:

$$\begin{cases} U_{sd} = R_{s\,I_{sd}} + \frac{d\psi_{sd}}{dt} - \omega_1\psi_{sq} \\ U_{sq} = R_{s\,I_{sq}} + \frac{d\psi_{sq}}{dt} + \omega_1\psi_{sd} \end{cases} \quad (2)$$

$$\begin{cases} \psi_{sd} = L_s\, I_{sd} + L_m I_{rd} \\ \psi_{sq} = L_s\, I_{sq} + L_m I_{rq} \end{cases} \quad (3)$$

Rotor:

$$\begin{cases} U_{rd} = R_r\, I_{rd} + \frac{d\psi_{rd}}{dt} - (\omega_1 - \omega_r)\psi_{rq} \\ U_{rq} = R_r\, I_{rq} + \frac{d\psi_{rq}}{dt} + (\omega_1 - \omega_r)\psi_{rd} \end{cases} \quad (4)$$

$$\begin{cases} \psi_{rd} = L_m\, I_{sd} + L_r I_{rd} \\ \psi_{rq} = L_m\, I_{sq} + L_r I_{rq} \end{cases} \quad (5)$$

where U_{sd} and U_{sq} are the d-axis and q-axis stator voltage parts, individually, R_s is the stator resistance, and I_{sd} and I_{sq} are d-axis and q-axis stator current segments, individually. Ψ_{sd}/ψ_{sq} is the stator flux linkage vector, ω_1 the synchronous speed, ω_r the rotor speed, L_s is the stator inductance, and L_m is the magnetizing inductance. s and r in the subscript recognize amounts or parameters on the stator or rotor side.

2.1.3. ROTOR SIDE CONVERTER (RSC) &GRID SIDE CONVERTER (GSC): The general structure of a two-level voltage source converter (VSC) is delineated in Fig. 2 (a). u_{sabc} is the three-phase voltage of the ac system. U_{cabc} is the three-phase ac side voltage of the VSC. I_{sabc} and i_{cabc} are the three-phase current. u_{dc}, i_d, and i_{dc} are the dc voltage, dc current, and dc side current of the VSC, individually. C_{dc} is the dc interface capacitor. To streamline the investigation, an average-value model of the two level VSC, as appeared in Fig. 2(b), is used for the RSC and GSC This model not just has practically indistinguishable enduring state and elements in low frequency with the point by point model, but also can significantly improve the simulation speed. In Fig. 2 (b), u_{sa},u_{sb}, and u_{sc} are the three-phase components of u_{sabc}. u_{ca},u_{cb}, and u_{cc} are the three-phase components of the equivalent controlled voltage u_{cabc}. R and L are the equivalent resistance and inductance, respectively.

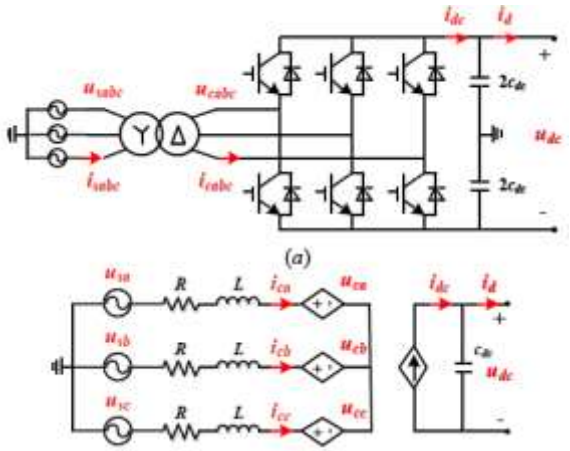

Fig. 2 Structure of the two-level VSC. (a) Detailed model. (b) Average-value model.

The relationship between u_{ca},u_{cb}, and u_{cc} and the ac voltage modulation indices m_a, m_b, and m_c are

$$u_{ca} = \frac{m_a u_{dc}}{2}, u_{cb} = \frac{m_b u_{dc}}{2}, u_{cc} = \frac{m_c u_{dc}}{2} \quad (6)$$

Ignoring the converter losses, the active power balance gives

$$i_{dc} = \frac{m_a\, i_{ca} + m_b i_{cb} + m_c i_{cc}}{2} \quad (7)$$

2.2. DVR

The DVR is a VSC connected at the WTG's terminal and in series with the power line via three single-phase ideal transformers to correct the deteriorated grid voltages. Further, the dc side of the DVR is connected to the dc link of the WTG. Another important component of DVR is the LC filter.

2.2.1. IDEAL TRANSFORMER: For an ideal transformer, the voltage and current in the primary and secondary sides are respectively given by:

$$\begin{cases} V_c = V_s - V_g \\ I_c = -I_g \end{cases} \quad (8)$$

Where V_c is the compensation voltage, V_g is the grid voltage, and V_s is the WTG's terminal voltage.

2.2.2. LC FILTER: The mathematical model of the LC filter can be obtained as

$$\begin{cases} V_f = L_{dvr}.\frac{dI_f}{dt} + V_c \\ I_f = C_{dvr} * \frac{dv_c}{dt} + I_c \end{cases} \quad (9)$$

Where I_c is the compensation current, I_f is the current generated by the DVR, and L_{dvr} and C_{dvr} are the filter parameters

2.2.3. DVR SIDE CONVERTER (DSC): The model of the DVR side converter (DSC) can also refer to the average-value model of the two-level VSC in Fig. 2(b).

2.3. ESS

A vanadium redox flow battery (VRB) based ESS is utilized in parallel association with the dc connection of the WTG with the DVR through a DC/DC converter.

2.3.1. VRB: The VRB is appropriate for WECS applications due to its enormous capacity, long life, low material cost, low support prerequisites, and quick reaction. The regular VRB model is in view of an identical circuit, which considers the physical and mathematical characteristics, as appeared in Fig. 3

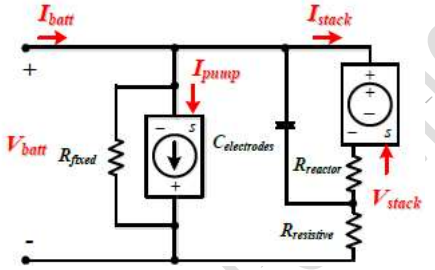

Fig. 3 Equivalent circuit model of VRB

The proposed model has the accompanying qualities [11]: 1) the SOC is displayed as a dynamically refreshed variable; 2) the stack voltage V_{stack} is displayed as a controlled voltage source, and the power moving through this source will affect the SOC; 3) as a controlled current source, the variable pump loss model, which is constrained by the pump loss current I_{pump}, is identified with the SOC and the current I_{stack} flowing through the battery stack. The VRB power loss incorporate two sections: one is from the comparable internal resistance, $R_{reactor}$ and $R_{resistive}$, and the other is the parasitic loss because of the parasitic fixed resistance and the pump loss. $C_{electrodes}$ is the electrode capacitance utilized to show the transient procedure.

2.3.2. DC/DC CONVERTER: A DC/DC converter is utilized to coordinate the VRB-based ESS, and the circuit diagram is depicted as follows.

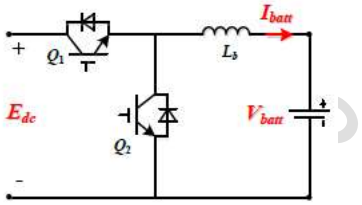

Fig. 4 Bidirectional DC/DC Converter

Where Q1 and Q2 are the power switches and L_b is the inductance.

3. CONTROL SCHEME FOR THE NOVEL WECS

From the general layout of the WECS in Fig. 1, four power conversion systems (RSC, GSC, DSC, and DC/DC converter) are employed. Detailed control schemes for each converter are illustrated in Fig. 5.

3.1. RSC

The RSC is designed to control the active and reactive power outputs of the stator P_s and Q_s. Independent control can be achieved through the rotor current control in the d-q reference frame. Assume that the stator flux ψ_s aligns with the d-axis, i.e.,

$$\begin{cases} \psi_{sd} = \psi_s \\ \psi_{sq} = 0 \end{cases} \quad (10)$$

Irrespective of the stator resistance Rs and the change of stator flux in steady state, the power outputs of the stator Ps and Qs are dependent on the q-axis rotor current I_{rq}, and the d-axis rotor current I_{rd}, respectively

$$\begin{cases} I_{rdref} = \left(K_{Qsp} + \frac{1}{K_{Qsi.s}} \right).(Q_{sref} - Q_s) \\ I_{rqref} = \left(K_{psp} + \frac{1}{K_{psi.s}} \right).(P_{sref} - P_s) \end{cases} \quad (11)$$

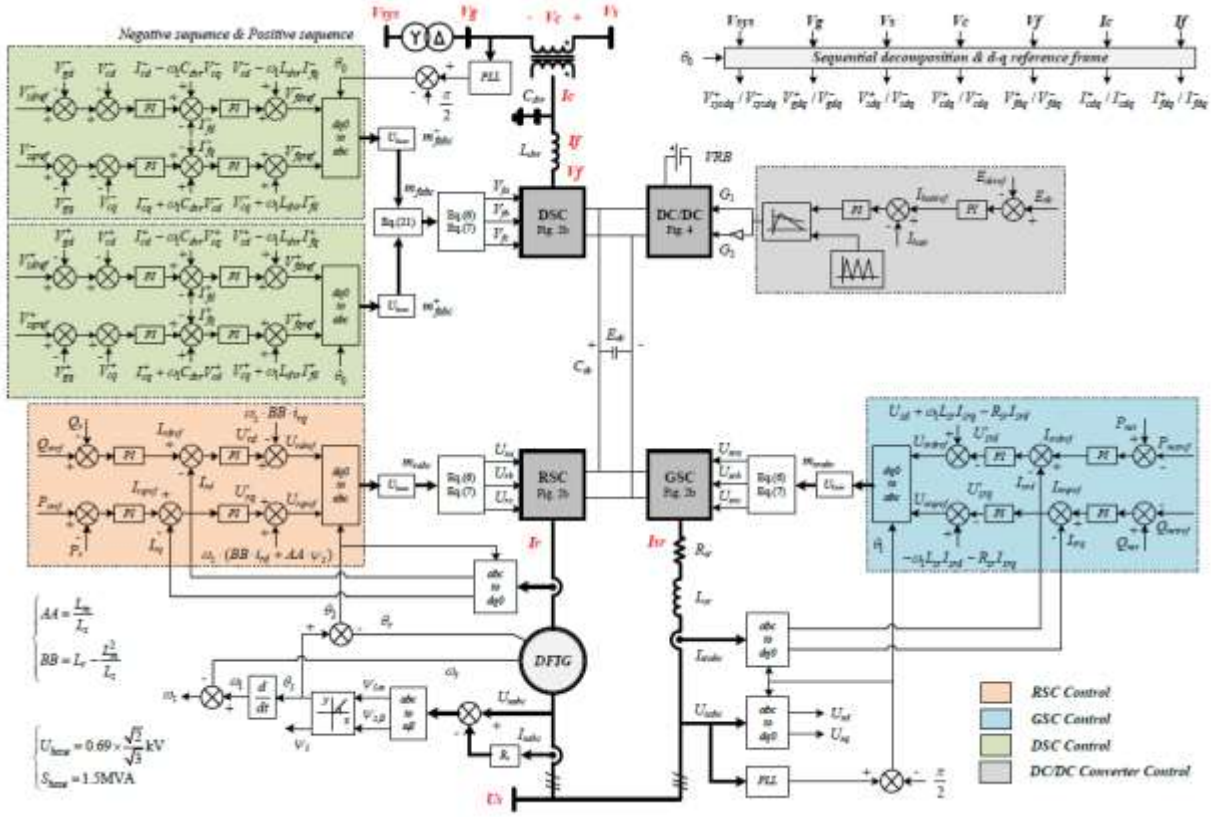

Fig. 5 Schematic diagram of the control system

The rotor currents are determined by the rotor voltages, and the relationship between them is:

$$\begin{cases} U_{rd} = U'_{rd} - \omega_s . BB . i_{rq} \\ U_{rq} = U'_{rq} + \omega_s \left(BB . i_{rd} + AA . \psi_s \right) \end{cases} \quad (12)$$

where AA=L_m/L_s, BB=L_r-L^2_m/L_s, and

$$\begin{cases} U'_{rd} = \left(K_{Irdp} + \frac{1}{K_{Irdi} . s} \right) . \left(I_{rdref} - I_{rd} \right) \\ U'_{rq} = \left(K_{Irqp} + \frac{1}{K_{Irqi} . s} \right) . \left(I_{rqref} - I_{rq} \right) \end{cases} \quad (13)$$

Finally, the reference rotor voltages (U_{rdref} and U_{rqref}) generated by the RSC are used to feed the WTG's rotor.

3.2. GSC

The function of the GSC is to control the active and reactive power outputs P_{net} and Q_{net} of the DFIG-WTG, respectively. In the same way, the independent control can be realized by the GSC current control in the d-q reference frame. Assume that the stator voltage U_s is aligned with the d-axis, i.e.

$$\begin{cases} U_{sd} = U_s \\ U_{sq} = 0 \end{cases} \quad (14)$$

Then, the power outputs P_{net} and Q_{net} of the DFIG-WTG are related to the d-axis grid-side current I_{srd}, and the q-axis grid-side current I_{srq}, respectively.

$$\begin{cases} I_{sdref} = \\ \quad \left(K_{pnetp} + \frac{1}{K p_{neti} . s} \right) * \left(P_{net} - P_{netref} \right) \\ I_{srqref} = \\ \quad \left(K_{Qnetp} + \frac{1}{K_{Qneti} . s} \right) * \left(Q_{net} - Q_{netref} \right) \end{cases} \quad (15)$$

The grid-side currents are determined by the grid-side voltages, and their relationship is:

$$\begin{cases} U_{srd} = U_{sd} - U''_{srd} + \omega_1 L_{sr} I_{srq} - R_{sr} I_{srd} \\ U_{srq} = -U'_{srq} - \omega_1 L_{sr} I_{srd} - R_{sr} I_{srq} \end{cases} \quad (16)$$

where R_{sr} and L_{sr} are the respective filter parameters,

and

$$\begin{cases} U'_{srd} = \left(K_{Isrdp} + \frac{1}{K_{Isrdi}.S}\right) * \left(I_{srdref} - I_{srd}\right) \\ U'_{srq} = \left(K_{Isrqp} + \frac{1}{K_{Isrqi}.S}\right) * \left(I_{srqref} - I_{srq}\right) \end{cases} \quad (17)$$

At long last, the reference network side voltages (U_{srdref} and U_{srqref}) are created by the GSC.

3.3. DSC

The point of the DVR is to rapidly remunerate the grid voltage unsettling influences and keep up the ideal WTG's terminal voltage. Because the majority of faults in the power system are unbalanced which results in unbalanced voltages. After the sequence decomposition, the positive and negative sequence vectors of V_{sys}, V_g, V_s, V_c, V_f, I_c, and I_f can be obtained as V^+_{sys}/V^-_{sys}, V^+_g/V^-_g, V^+_s/V^-_s, V^+_c/V^-_c, V^+_f/V^-_f, I^+_c/I^-_c, and I^+_f/I^-_f, respectively. Then based on the d-q reference frame, the d-axis and q-axis components can be respectively derived as V^+_{sysdq}/V^-_{sysdq}, V^+_{gdq}/V^-_{gdq}, V^+_{sdq}/V^-_{sdq}, V^+_{cdq}/V^-_{cdq}, V^+_{fdq}/V^-_{fdq}, I^+_{cdq}/I^-_{cdq}, and I^+_{fdq}/I^-_{fdq}. The positive sequence vector of the grid voltage Vg is assumed to align with the d-axis, i.e., $V^+_{gd} = V^+_g$, $V^+_{gq} = 0$. Note that the rotation direction of the positive sequence vector and the negative sequence vector are opposite. The injected compensated voltages must be figured carefully with the goal that the WTG's terminal voltages are well compensated regarding the pre-sag voltages. The reference of the compensated voltage over the ideal transformer can be expressed as follows:

$$\begin{cases} V^*_{cdref} = V^*_{sdref} - V^*_{gd} \\ V^*_{cqref} = V^*_{sqref} - V^*_{gq} \end{cases} \quad (18)$$

where V^*_{sdref} and V^*_{sqref} are the pre-sag terminal voltages, V^*_{gd} and V^*_{gq} are the grid voltages after the voltage sag occurs, and the superscript "*" denotes the positive (+) or negative (-) sequence components. From (9), the controller designed for the DSC is depicted as

$$\begin{cases} V^*_{fd} = L_{dvr}.\frac{dI^*_{fd}}{dt} - \omega_1 L_{dvr} I^*_{fq} + V^*_{cd} \\ V^*_{fq} = L_{dvr}.\frac{dI^*_{fq}}{dt} + \omega_1 L_{dvr} I^*_{fd} + V^*_{cq} \\ I^*_{fd} = C_{dvr}.\frac{dv^*_{cd}}{dt} - \omega_1 c_{dvr} v^*_{cq} + I^*_{cd} \\ I^*_{fq} = C_{dvr}.\frac{dv^*_{cq}}{dt} + \omega_1 c_{dvr} v^*_{cd} + I^*_{cq} \end{cases} \quad (19)$$

Based on (18) and (19), the voltage reference can be derived in the d-q reference frame as

$$\begin{cases} V^*_{fdref} = \left(K_{Ifdp} + \frac{1}{K_{Ifdi}.S}\right) * \left(I^*_{fdref} - I^*_{fd}\right) - \omega_1 L_{dvr} I^*_{fq} + V^*_{cd} \\ V^*_{fqref} = \left(K_{Ifqp} + \frac{1}{K_{Ifqi}.S}\right) * \left(I^*_{fqref} - I^*_{fq}\right) + \omega_1 L_{dvr} I^*_{fd} + V^*_{cq} \\ I^*_{fdref} = \left(K_{vcdp} + \frac{1}{K_{Ifdi}.S}\right) * \left(V^*_{cdref} - V^*_{cd}\right) - \omega_1 C_{dvr} V^*_{cq} + I^*_{cd} \\ I^*_{fqref} = \left(K_{vcqp} + \frac{1}{K_{vcqi}.S}\right) * \left(V^*_{cqref} - V^*_{cq}\right) + \omega_1 C_{dvr} V^*_{cd} + I^*_{cq} \end{cases} \quad (20)$$

After the reference voltage of the DSC is determined, the positive and negative succession segments in the d-q reference outline are changed to the stationary abc reference casing and afterward added, as given by

$$\begin{cases} m_{fa} = m^+_{fa} + m^-_{fa} \\ m_{fb} = m^+_{fb} + m^-_{fc} \\ m_{fc} = m^+_{fc} + m^-_{fb} \end{cases} \quad (21)$$

3.4. DC/DC CONVERTER

The bi-directional DC/DC converter is an interface planned to move vitality between the VRB based ESS and the dc connect of the WTG. Its control target is to keep up the dc connect voltage E_{dc}. The control conspire contains two cascaded control loops. The deliberate voltage E_{dc} is contrasted and the reference E_{dcref} and the blunder is conveyed to the external loop PI voltage controller, which creates a present reference $I_{battref}$ for the internal loop PI current controller. The present controller looks at $I_{battref}$ to the deliberate ESS current I_{batt} so as to create gating signals for the IGBT switches. At last, the

DC/DC converter charges or releases the VRB based ESS as per the obligation proportion of the two IGBT switches Q1 and Q2.

4. FUZZY LOGIC CONTROLLER

Conventional controllers require complex mathematical modeling which involves complex mathematical equations. On the other hand, fuzzy logic controller doesn't involve any complex mathematical modelling and can be easily modeled for nonlinear systems. In fuzzy logic controller, operational laws are in terms of linguistic terms rather than simple mathematical equations. There exist many complex controllers where it be difficult to model them accurately. So, it is better to employ fuzzy logic for nonlinear controllers as they are easier and much more feasible.

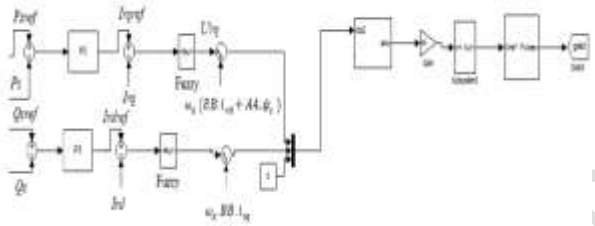

Fig. 6 Control scheme of RSC with Fuzzy controller

The modelling of fuzzy logic controller involves: 1) Input and output both have seven fuzzy sets. 2) Fuzzification of inputs using continuous universe of discourse. 3) Connotation using Mamdani's 'min' operator. 4) 'Centroid' method used for defuzzication.

Triangular membership function is based on equation of straight line which for the ease of computation is used to design fuzzy sets. This triangular curve can be represented as

$$\mu_A(x) = \max\left(min\left(\frac{x-a}{c-a}, \frac{c-x}{c-b}\right), 0\right) \qquad (22)$$

Here 'e' indicates error and 'ce' indicates change in error and are two inputs of fuzzy system. The output of fuzzy is rotor voltage as shown in Fig.6. The fuzzy rule table with seven input and output fuzzy set is given below.

Table I. Fuzzy controller rules

e/ce	NB	NM	NS	ZE	PS	PM	PB
NB	NB	NB	NB	NB	NM	NS	ZE
NM	NB	NB	NB	NM	NS	ZE	PS
NS	NB	NB	NM	NS	ZE	PS	PM
ZE	NB	NM	NS	ZE	PS	PM	PB
PS	NM	NS	ZE	PS	PM	PB	PB
PM	NS	ZE	PS	PM	PB	PB	PB
PB	ZE	PS	PM	PB	PB	PB	PB

Both 'e' and 'ce' i.e. rotor current error and change in rotor current error respectively are measured continuously and given as input to the fuzzy block in Simulink model of RSC as shown in Fig.6. When compared to the trapezoidal membership functions, the triangular membership functions have advantage of simplicity in construction. Hence triangular membership function is used in this paper. The seven membership functions are represented as 'NB'-Negative Big, 'NM'-Negative Medium, 'NS'-Negative Small, 'ZE'-Zero, 'PS'-Positive Small, 'PM'-Positive Medium, 'PB'-Positive Big. On the basis of different range of values for 'e' and ' ce', the discrimination of membership functions are done. The input triangular membership functions 'e' and 'ce' and output are shown Fig.7.

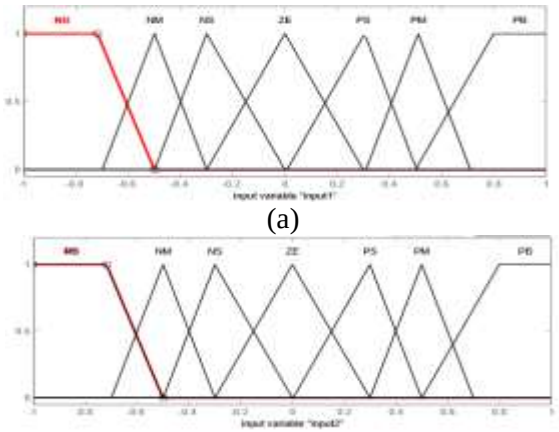

(a)

(b)

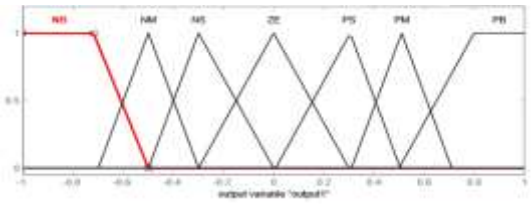

(c)

Fig.7 Membership functions (a) Error (b) Change in error and (c) output

5. SIMULATION RESULTS

A novel double fed induction generator (DFIG)-based wind-energy conversion system (WECS) by using fuzzy logic controller is modeled as shown in Fig.8. In this system, the fault operation conditions are simulated to test the system performance.

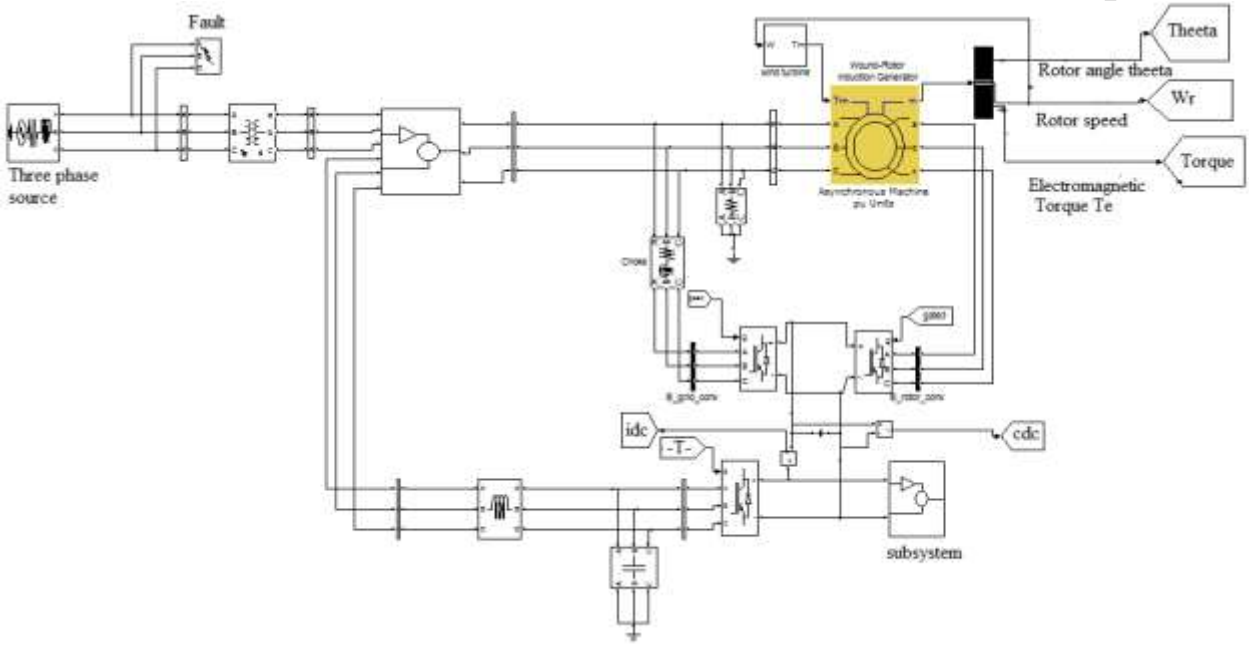

Fig. 8 Simulink model of the novel DVR-ESS-embedded WECS

5.1. FAULT OPERATION CONDITION

Case 1: Symmetrical grid fault (50% voltage dip)

The performance of the DVR-ESS-embedded WECS by using fuzzy logic controller under symmetrical grid fault is given in Fig.9. When a balanced voltage disturbance occurs in the grid at 0.05s as shown in Fig.9 (a), the DVR generates the compensation voltage V_c in very less time, as result the WTG's terminal voltage V_s can be maintained in limits as shown in Fig.9 (c). In Fig.9 (d), the rms currents of the RSC and GSC are maintained at below 500 ampere during disturbance. The *SOC* of the VRB is shown in Fig.9 (e). It decreases when the VRB discharges during the initial 0.05s, and then the SOC continues to increase. Even under severe voltage disturbance condition in the grid the dc link voltage V_{dc} is slightly affected because of the DVR compensation as depicted in the fig.9 (f). It can be observed that the generated wind power P_{net} is slightly altered, the grid connected power P_{wind} is reduced, due to which the surplus power P_{dvr} is absorbed by VRB as shown in fig.9 (g). This is expected as part of stored generation power, which can be used for suppressing wind power fluctuations without any loss of wind power generation.

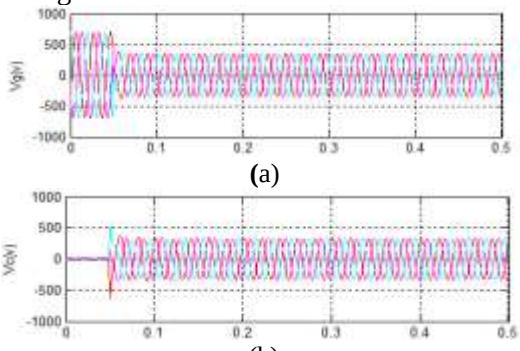

(a)

(b)

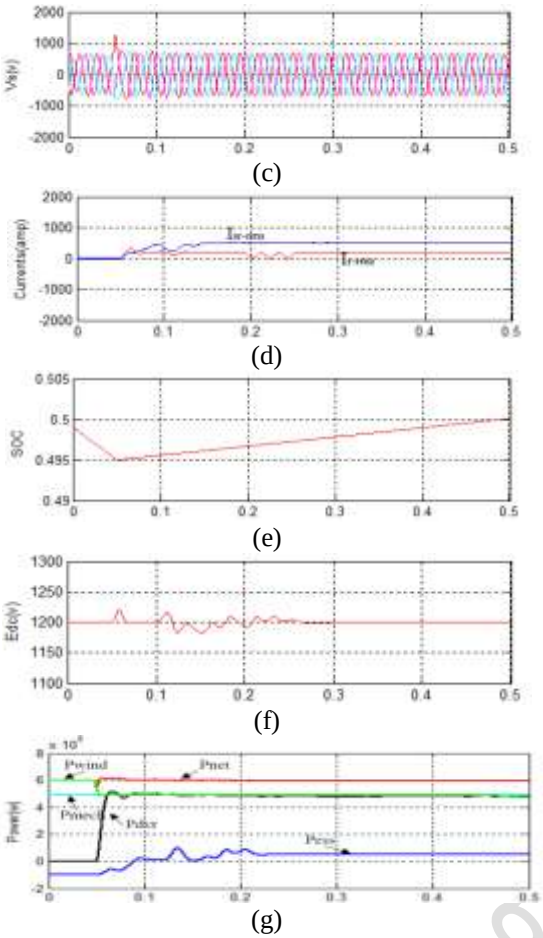

Fig. 9 Symmetrical grid fault with 50% voltage dip. (a) Grid voltage (b) Compensation voltage (c)WTG's terminal voltage (d) RSC/GSC current RMS (e) State of charge (f)) DC link voltage (g) Power response.

Case 2: Symmetrical grid fault (90% voltage dip)

In this case, the scenario with 90% voltage dip is simulated. The fault occurs at 0.05s in Fig.10 (a). The DVR compensates the voltage dip quickly in Fig.10 (b) to restore the system voltage of the wind turbine in Fig.10 (c). The current of the converter can be limited in 500 ampere in Fig.10 (d). Large power fluctuation is suppressed by the energy storage system in Fig.10 (g). It can be observed that VRB discharges to generate the compensation power during the initial 0.05s and then the SOC continue to increase as shown in Fig.10 (e). The dc-link voltage experiences oscillation but it can be controlled with the support of the control scheme.

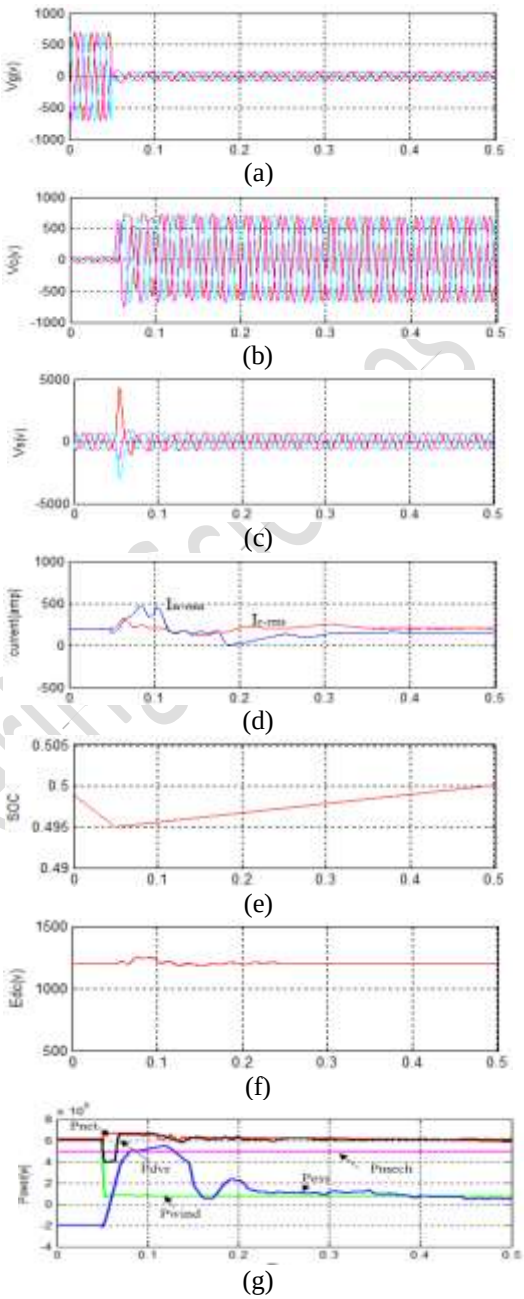

Fig. 10 Symmetrical grid fault with 90% voltage dip. (a) Grid voltage. (b) Compensation voltage. (c) WTG's terminal voltage. (d) RSC/GSC current RMS. (e) State of charge. (f) DC link voltage. (g) Power response.

Case 3: Asymmetrical grid fault (50% voltage dip)

A single phase to ground fault with 50% voltage dip was simulated. To be specific phase A in V_{sys} is grounded at 0.55 sec. Because of the transformer is in DY11 connection, the

magnitude of phase A and phase B in grid voltage V_g decreases respectively as shown in fig.11 (a). As the compensation voltage V_c generated by the DVR in fig.11 (b), the WTG's terminal voltage V_s can be maintained at its rated value as depicted in fig.11 (c). The rms currents of the GSC and RSC are kept below at 500 amperes as shown in fig.11 (d). The SOC of VRB is shown in fig.11 (e). The VRB has to be absorb more wind power after the single line to ground fault takes place. In the same way, the DC/DC converter keeps the dc link voltage E_{dc} stable even under asymmetrical grid disturbance as shown in fig.11 (f). The generated wind power P_{net} is slightly affected by the asymmetrical grid fault. As the positive sequence vector in V_g is reduced, the grid connected power P_{wind} is also reduced as well, and the remaining power generation P_{dvr} has to be absorbed by VRB is depicted in fig.11 (g).

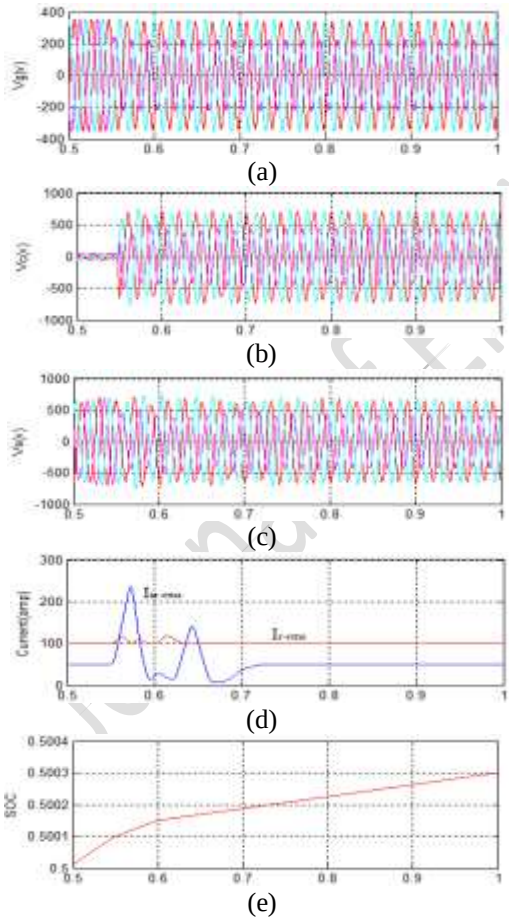

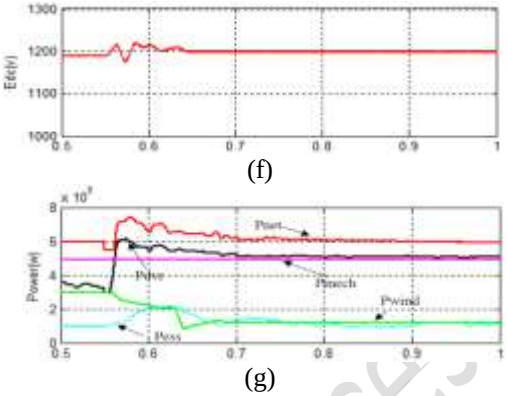

Fig. 11 Asymmetrical grid fault with 50% voltage dip. (a) Grid voltage. (b) Compensation voltage. (c) WTG's terminal voltage. (d) RSC/GSC current RMS. (e) State of charge. (f) DC link voltage. (g) Power response.

5.2. COMPARISION OF THD FOR PI AND FUZZY CONTROL SCHEME

This case is simulated to test the system performance of proposed FL based WECS for total harmonic distortion (THD) improvement. The THD values of different voltages at different cases are shown in Table II.

Table II. %THD values of different voltages at different cases

	Case 1		Case 2		Case 3	
	PI	Fuzzy	PI	Fuzzy	PI	Fuzzy
V_g	1.35	0.34	1.76	0.88	2.19	1.10
V_s	2.15	1.06	8.5	2.94	1.47	1.39
V_c	2.01	1.81	4.18	2.24	0.85	0.8

In case 1 with PI controller the %THD in grid voltage V_g , system voltage V_s and compensation voltage V_c is 1.35%, 2.15% and 2.01% and with Fuzzy controller these were reduced to 0.34%, 1.06% and 1.81% respectively. Thus, the proposed Fuzzy logic controller has effectively reduced the THD compared to PI controller scheme. The THD values of the case 1 for both controllers are shown in Fig. 12, 13 & 14.

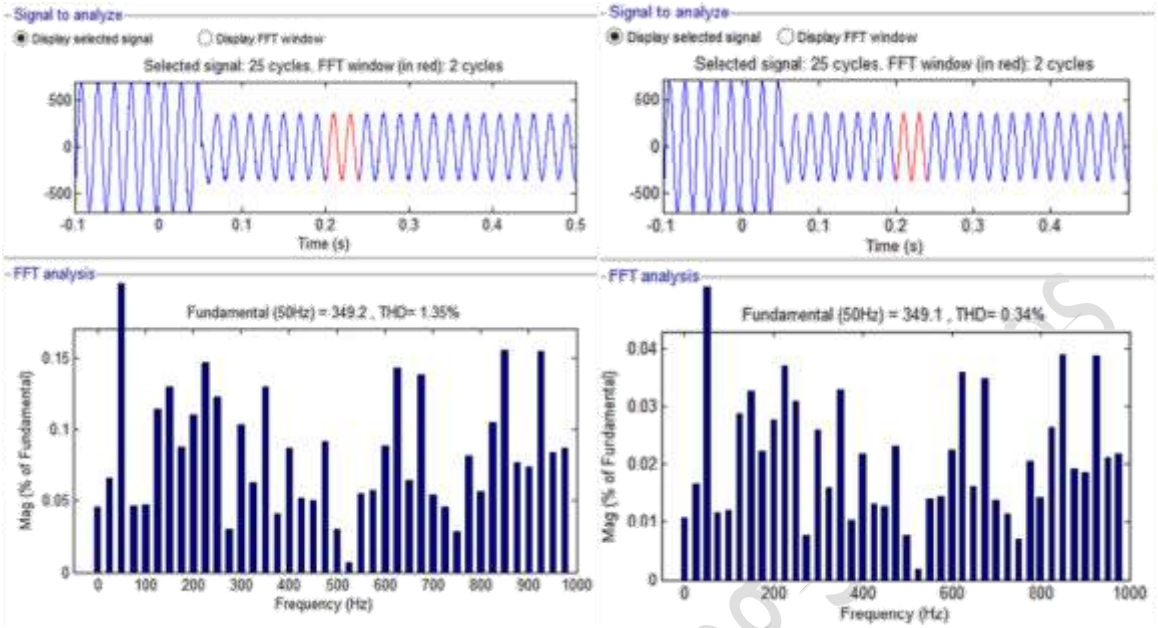

Fig.12 (a) %THD value of V_g for PI controller, (b)%THD value of V_g for Fuzzy controller.

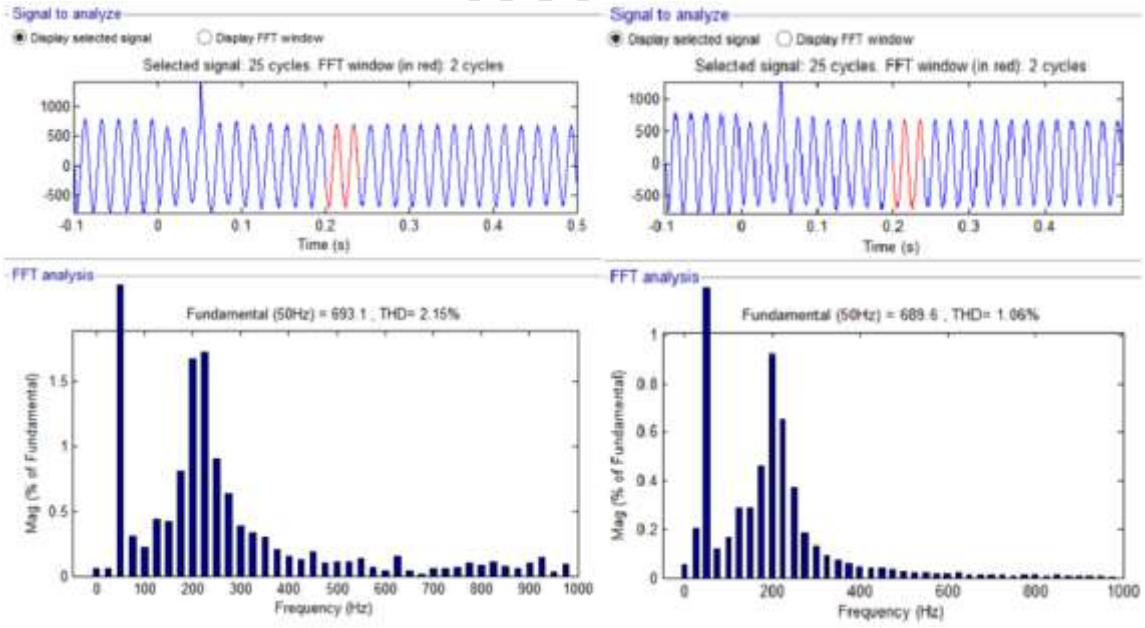

Fig. 13 (a) %THD value of V_s for PI controller, (b) %THD value of V_s for Fuzzy controller.

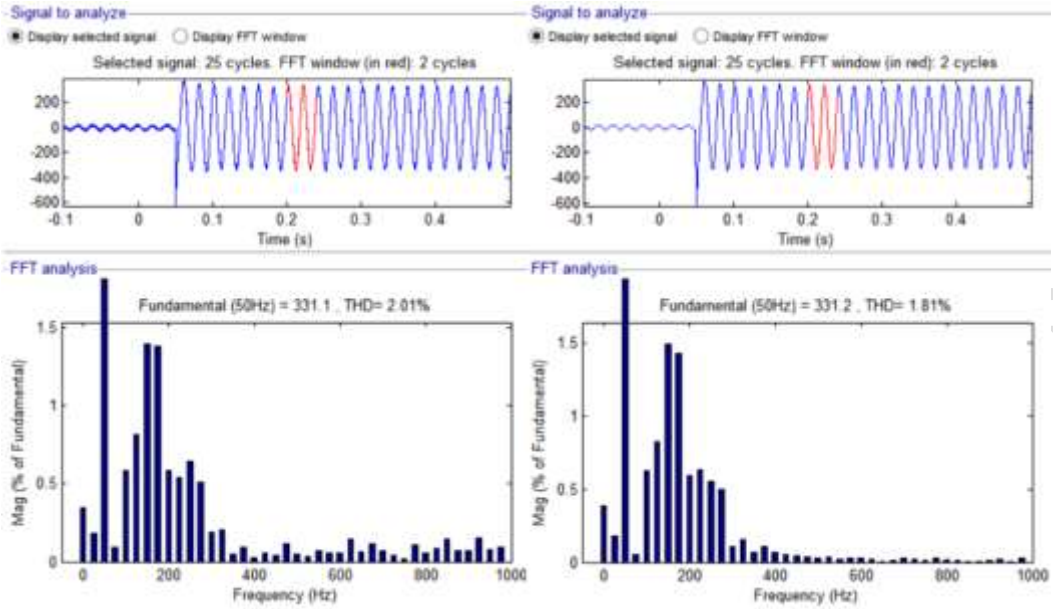

Fig. 14 (a) %THD value of V_c for PI controller, (b) %THD value of V_c for Fuzzy controller.

6. CONCLUSION

A novel DVR-ESS embedded WECS by using fuzzy logic controller is proposed. The ESS can store surplus wind power for discharge when required and it can adequately suppress wind power fluctuations and further improve the penetration level of wind power. The DVR can altogether improve the FRT ability of the WECS under symmetrical and asymmetrical fault conditions. In order to see the performance of each individual control scheme, symmetrical fault with 50% sag, 90% sag and asymmetrical fault with 50% sag was simulated. It was observed that fuzzy control scheme gave less THD content in V_g, V_s and V_c when compared to PI control scheme. It also improves the dynamic response of the system.

REFERENCES

[1] T. Ackermann, Wind Power in Power Systems,2nd ed., Chichester: Wiley-Blackwell, 2012.

[2] International Electrotechnical Commission, Grid integration of large capacity renewable energy sources and use of large capacity electrical energy storage, White paper, 2012.

[3] A. McDonald and G. Jimmy, Parallel wind turbine powertrains and their design for high availability, IEEE Trans. Sustain. Energy, vol. 8, no. 2, pp. 880-890, Apr. 2017.

[4] J. Yao, H. Li, Z. Chen, X, Xia, X, Chen, Q, Li, and Y, Liao, Enhanced control of a DFIG-based wind-power generation system with series grid-side converter under unbalanced grid voltage conditions, IEEE Trans. Power Electron., vol. 28, no.7, pp. 3167-3181, Jul. 2013.

[5] S. Alaraifi, A. Moawwad, M. S. El Moursi, and V. Khadkikar, Voltage booster schemes for fault ride-through enhancement of variable speed wind turbines, IEEE Trans. Sustain. Energy, vol. 4, no. 4, pp. 1071– 1081, Oct. 2013

[6] P. S. Flannery, and G. Venkataramanan, A fault tolerant doubly fed induction generator wind turbine using a parallel grid side rectifier and series grid side converter, IEEE Trans. Power Electron., vol. 23, no. 3, pp. 1126-1135, May. 2008.

[7] Y. Q. Zhang, Z. Chen, W. H. Hu and M. Cheng, Flicker mitigation by individual pitch control of variable speed wind turbines with DFIG, IEEE Trans. Energy Convers., vol. 29, no. 1, pp. 20-28, Mar. 2014.

[8] T. Senjyu, R. Sakamoto N. Urasaki, T. Funabashi, H. Fujita and H. Sekine, Output power leveling of wind turbine generator for all operating regions by pitch angle control, IEEE Trans. Energy Convers., vol. 21, no. 2, pp. 467-475, Jun. 2006.

[9] E. Kamal, A. Aitouche, R. Ghorbani, and M. Bayart, Robust fuzzy faulttolerant control of wind energy conversion systems subject to sensor

faults, IEEE Trans. Sustain. Energy, vol. 3, no. 2, pp. 231–241, Apr. 2012.

[10] [10] C. L. Luo, H. Banakar, B. Shen, B. Ooi, Strategies to smooth wind power fluctuations of wind turbine generator, IEEE Trans. Energy Convers., vol. 22, no. 2, pp. 341-349, Jun. 2007

[11] X. Chen, L. Wang, H. Sun, and Y. Chen, Fuzzy logic based adaptive droop control in multi-terminal HVDC for wind power integration, IEEE Trans. Energy Convers., vol. 32, no. 3, pp. 1200-1208, Sept. 2017.

[12] J. P. Barton, D. G. Infield, Energy Storage and Its Use with Intermittent Renewable Energy," IEEE Trans. Energy Converters., vol. 19, no. 2, pp. 441-448, Jun. 2004.

[13] W. Qiao, G. K. Venayagamoorthy and R. G. Harley, real-time implementation of a STATCOM on a wind farm equipped with doubly fed induction generators, IEEE Trans. Ind. App., vol. 45, no. 1, pp. 98-107, Feb. 2009.

[14] Y. W. Shen, D. P. Ke, W. Qiao, Y. Z. Sun, D. S. Kirschen and C. Wei, "Transient reconfiguration and coordinated control for power converters to enhance the LVRT of a DFIG wind turbine with an energy storage device, IEEE Trans. Energy Convers., vol. 30, no. 4, pp. 1679-1690, Dec. 2015.

[15] S. Kuenzel, L. P. Kunjumuhammed, B. C. Pal, and I. Erlich, Impact of wakes on wind farm inertial response, IEEE Trans. Sustain. Energy, vol. 5, no. 1, pp. 237–245, Jan. 2014.

[16] J. Lee, E. Muljadi, P. Sorensen, and Y. C. Kang, "Releasable kinetic energy-based inertial control of a DFIG wind power plant," IEEE Trans. Sustain. Energy, vol. 7, no. 1, pp. 279–288, Jan. 2016.